Non-ideal Gas Effects
on Supersonic-Nozzle Transfer Functions

Stephen D. Winn[1,2(✉)] and Emile Touber[1,2]

[1] Department of Mechanical Engineering, Imperial College London, London, UK
stephen.winn16@imperial.ac.uk
[2] Shocks, Solitons and Turbulence Unit, Okinawa Institute of Science
and Technology, Okinawa, Japan
emile.touber@oist.jp

Abstract. Flow disturbances traveling in a nozzle can be amplified or attenuated and generate excessive acoustic noise (e.g. jet engine exhaust) or interact with shocks to cause excessive loading on components (e.g. between turbine blades). Non-ideal gas-dynamic effects are investigated within the framework of linearised inviscid quasi-one dimensional nozzle flow. The transfer function of choked supersonic divergents is investigated when prescribing an inlet entropy perturbation. Initial results using a van der Waals gas highlight the contrast with ideal gas behaviour with and without a shock in the divergent. For the chosen conditions, in the shock-free configuration, a five-fold increase in amplification of pressure perturbations at higher wavelengths (relative to nozzle length) and stronger attenuation (over one order of magnitude lower) at lower wavelengths is observed when compared to an ideal gas. In the shocked configuration, greater amplification is again observed in the van der Waals case owing to the selectivity of the shock in amplifying the incoming density perturbations. Furthermore, up to an order of magnitude greater shock displacement is observed over the range of perturbation wavelengths in the van der Waals case.

Keywords: Transfer function · Quasi-one dimensional nozzle flow · Non-ideal gas effects · Thermodynamic critical point · Dense gas

1 Linearised Quasi-One Dimensional Nozzle Flow

The equations governing the flow herein are the inviscid, quasi-one dimensional Euler equations:

$$\frac{\partial}{\partial t} \begin{bmatrix} \rho \\ \rho u \\ \rho e_t \end{bmatrix} + \frac{\partial}{\partial x} \begin{bmatrix} \rho u \\ \rho u^2 + p \\ u(\rho e_t + p) \end{bmatrix} + \frac{1}{A}\frac{\mathrm{d}A}{\mathrm{d}x} \begin{bmatrix} \rho u \\ \rho u^2 \\ u(\rho e_t + p) \end{bmatrix} = \begin{bmatrix} 0 \\ 0 \\ 0 \end{bmatrix}, \qquad (1)$$

where ρ, u, p, e_t are, respectively, the fluid density, velocity, pressure, total energy (where $e_t = e + u^2/2$) and A is the nozzle cross-section area. These are supplemented with the equation of state for internal energy, e, for an arbitrary gas.

An infinitesimal harmonic (in time) perturbation of the base-flow is considered for any of the primitive variables $q \in \{\rho, u, p\}$ such that:

$$q(x,t) = \bar{q}(x) + \epsilon q(x)' e^{i\omega t}, \tag{2}$$

where ω is the frequency of the perturbation ($\omega \in \mathbb{R}_{>0}$), ϵ is an arbitrarily-small non-dimensional parameter ($\epsilon \ll 1$) and $i^2 = -1$. Injecting this form in the governing equations and retaining only first order terms yields the linearised equations without any assumption on the gas model of the form:

$$\begin{bmatrix} \bar{u} & \bar{\rho} & 0 \\ 0 & \bar{u} & \frac{1}{\bar{\rho}} \\ 0 & \bar{\rho}c^2 & \bar{u} \end{bmatrix} \frac{\mathrm{d}\mathbf{q}'}{\mathrm{d}x} = \left(\frac{1}{(\bar{M}^2-1)A} \frac{\mathrm{d}A}{\mathrm{d}x} \begin{bmatrix} -\tilde{c}\bar{M}^3 & \bar{\rho} & 0 \\ \bar{M}^2\tilde{c}^2 & -\bar{M}\tilde{c} & 0 \\ -\bar{M}^3\tilde{c}^2\left(\tilde{c}+2\bar{\rho}\tilde{c}_\rho\right) & \bar{\rho}\tilde{c}^2 & -2\bar{M}^3\tilde{c}^2\tilde{c}_p\bar{\rho} \end{bmatrix} - i\omega\mathbf{I} \right) \mathbf{q}', \tag{3}$$

where $\mathbf{q}' = [\rho', u', p']^T$ is the vector of complex perturbation values, $\tilde{c} = c(\bar{\rho}, \bar{p})$ is the isentropic speed of sound, c, evaluated on the base-flow thermodynamic properties and $\tilde{c}_\rho = (\partial c/\partial \rho)_p (\bar{\rho}, \bar{p})$, $\tilde{c}_p = (\partial c/\partial p)_\rho (\bar{\rho}, \bar{p})$. These are supplemented with the Rankine–Hugoniot jump conditions and their linearised counter-part to relate fluctuations either side of a shock to the base-flow values and their gradients:

$$\begin{bmatrix} \bar{u}_b & \bar{\rho}_b & 0 \\ \bar{u}_b^2 & 2\bar{\rho}_b\bar{u}_b & 1 \\ -\left.\frac{\partial \wp}{\partial \rho}\right|_b & 0 & 1 \end{bmatrix} \begin{bmatrix} \rho_b' \\ u_b' \\ p_b' \end{bmatrix} + \begin{bmatrix} -i\omega[\![\bar{\rho}]\!] \\ \frac{\bar{\rho}_a^2\bar{u}_a^2}{A}\frac{\mathrm{d}A}{\mathrm{d}x}[\![\frac{1}{\bar{\rho}}]\!] \\ \left(\frac{\partial \wp}{\partial p}\frac{\mathrm{d}\bar{p}}{\mathrm{d}x} + \frac{\partial \wp}{\partial \rho}\frac{\mathrm{d}\bar{\rho}}{\mathrm{d}x}\right)\Big|_a + \left(\frac{\partial \wp}{\partial \rho}\frac{\mathrm{d}\bar{\rho}}{\mathrm{d}x} - \frac{\mathrm{d}\bar{p}}{\mathrm{d}x}\right)\Big|_b \end{bmatrix} x_s' = \begin{bmatrix} \bar{u}_a & \bar{\rho}_a & 0 \\ \bar{u}_a^2 & 2\bar{\rho}_a\bar{u}_a & 1 \\ \left.\frac{\partial \wp}{\partial \rho}\right|_a & 0 & \left.\frac{\partial \wp}{\partial p}\right|_a \end{bmatrix} \begin{bmatrix} \rho_a' \\ u_a' \\ p_a' \end{bmatrix}, \tag{4}$$

where x_s' is the shock displacement and $\wp = \wp(\rho, p, M)$ is the shock-adiabat pressure (such that $p_b = \wp(\rho_a, p_a, M_a)$), the derivatives of which are evaluated using the base-flow values at the locations shown in Fig. 2. Integrating Eq. 3 yields the spatial distribution of $\mathbf{q}'$ in a nozzle and thus the transfer function (modulus and phase at the outlet) resulting from any combinations of physical boundary conditions. A divergent with a linear increase in cross-section area (henceforth referred to as a linear nozzle) is employed to expand a gas from an initial strictly supersonic state (see schematic Fig. 3, left). Two cases are investigated: a shock free nozzle and a divergent containing a compression shock. It is assumed that the cross-section area is constant upstream and downstream of the linear nozzle. An inlet perturbation in the form of entropy and acoustic waves is prescribed. Such an analysis has been used for an ideal gas to provide useful insight into the transfer function of choked nozzles e.g. [2].

2 Non-ideal Gas Model

Non-ideal gas properties are explored herein using the van der Waals (vdW) gas equation. In the vicinity of the thermodynamic critical point (TCP), dense gases (i.e. gases that are characterised by a large ratio of specific heat, c_v to gas constant, R) present a region where the fundamental derivative of gas dynamics,
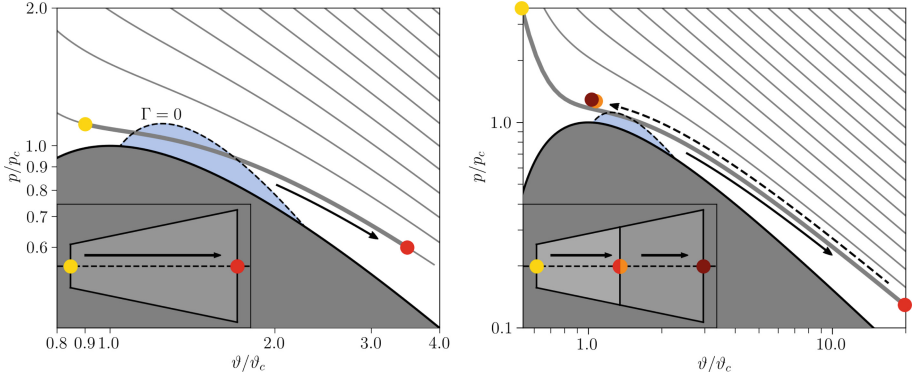
Fig. 1. $(p\text{-}\vartheta)$ diagrams for a van der Waals gas (with $R/c_v = 1.3 \times 10^{-2}$). Isentropes are shown in thin grey lines, with the region where they become concave ($\Gamma < 0$) shaded in light blue. The two-phased region is shown in dark-grey. Left: isentrope chosen for the supersonic expansion of Sect. 3.1. Right: supersonic expansion isentrope (yellow → red) and subsonic compression (orange → maroon) chosen for Sect. 3.2. A schematic of the corresponding locations in the nozzle is given in the bottom left.

$\Gamma \equiv 1 + (\rho/c)\,(\partial c/\partial \rho)_s$, can become negative (see Fig. 1) denoting locally concave isentropes. Admissible steady-state flows in this region have been explored and categorised (see e.g. [4]). For supersonic expansions close to the TCP, certain stagnation conditions lead to the Mach number having a non-monotonous behaviour as shown in Fig. 3 (left) which is impossible in ideal gases (we restrict ourselves to expansions that contain only one sonic point). Furthermore, the energy transfer properties of shocks in this region present an acute sensitivity to the upstream state and Mach number, explored in [1], and allow for a degree of control over the energy redistribution downstream of the shock. In Sects. 3 and 4, the computations are carried out using the van der Waals gas model and the ideal gas model for comparison. In both cases, the ratio $R/c_v = 0.013$ is used which is representative of PP10 gas [1].

3   Transfer Function of a Choked Supersonic Nozzle

The results for the transfer function of the supersonic nozzle is divided into two steps as illustrated in Fig. 2. First, results for the transfer function of a supersonic expansion alone are presented followed by the results with the addition of a shock in the divergent section.

3.1   Transfer Function of a Shock-Free Nozzle

For given thermodynamic inlet (subscript 1) and outlet states (subscript 2), the transfer function of a linear nozzle for a given inlet perturbation depends on two parameters: the mass flow through the nozzle, $\dot{m}$, and the ratio of the perturbation wavelength, λ, and the nozzle length, L. Figure 3 presents the transfer
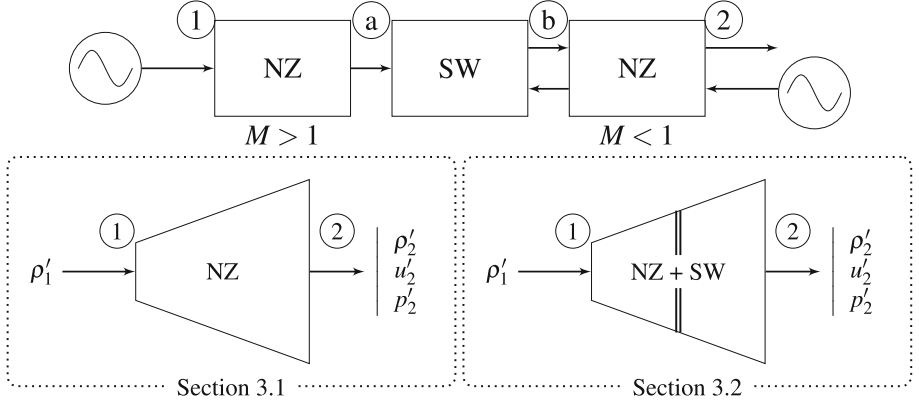
Fig. 2. Top: Schematic of the 'blocks' in the transfer function of a choked supersonic nozzle (NZ) containing a shock (SW). Bottom: shock-free and shocked nozzle 'blocks' with notations for the two configurations considered.

functions (in terms of modulus) for an inlet entropy perturbation over a range of λ/L values. The inlet perturbation generates greater ($\times 5$) pressure perturbation in the vdW case for larger wavelengths (relative to nozzle length). This is of interest, for example, when considering 'indirect noise' generation in turbines (i.e. acoustic noise generated from entropy perturbations [3]). Furthermore, at higher wavelength, the density perturbations undergo greater amplification in the vdW case than in the ideal gas case which could exacerbate the shock transfer effects discussed in following section (and [1]). However, for $\lambda \leq L$, the density and pressure perturbations are, over most of the range, attenuated in the vdW case compared to the ideal gas (e.g. at $\lambda/L = 0.1$, $|p'_{2,vdw}|/|p'_{2,ig}| \approx 0.2$ and $|\rho'_{2,vdw}|/|\rho'_{2,ig}| \approx 9 \times 10^{-2}$).

3.2   Transfer Function of a Shocked Nozzle

The addition of a shock in the nozzle requires specifying two additional boundary conditions: one is the exit thermodynamic state (state 2 in Fig. 2, bottom right) to determine where the post-shock subsonic compression ends. The other is the perturbation boundary conditions i.e. the magnitude and phase of upstream propagating acoustic wave at the exit of the nozzle. In the case presented here, there is no back-propagating forcing imposed at the exit of the nozzle. Furthermore, for the following results, the shock is placed at $\bar{x}_s = 2L/3$ thus determining the extent of the subsonic compression and the exit conditions. The shock configuration presented in this section was chosen based on the work carried out by [1]. In the isolated shock case, Alferez & Touber identified shock transmission properties allowing for a strong amplification of the entropy mode (up to two orders of magnitude greater than the ideal gas case). In the current configuration, presented in Fig. 4 (left), this overall amplification difference through the
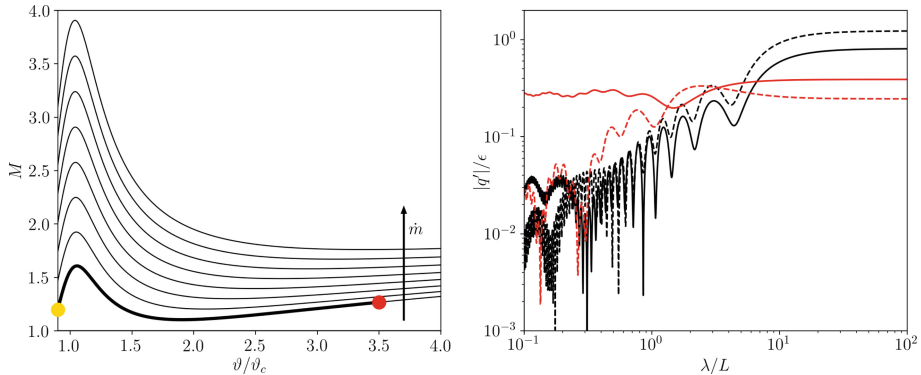
Fig. 3. Left: evolution of the Mach number along the thicker isentrope of Fig. 1 (left) $(s_0 = s(\bar{T}_0, \bar{p}_0)$, where $\bar{T}_0 = T_c$ and $\bar{p}_0 = 0.6 p_c)$ for various mass flows. The thicker line denotes $\dot{m}$ used in the shock-free case. Subscript c denotes critical point values. Right: Transfer function (modulus only) of the supersonic expansion along the thick isentrope given in Fig. 1 (left) with $M_1 = 1.2$ for an inlet entropy perturbation for various wavelengths. Solid and dashed lines are for $|\rho'_2/\epsilon|$ and $|p'_2/\epsilon|$ respectively, with red for ideal gas, black for vdW gas.

nozzle is comparable (the maximum ratio $|\rho'_{2,vdw}|/|\rho'_{2,ig}| \approx 149$ for $\lambda/L \approx 0.14$). For both ideal gas and vdW gases, the transfer function for the density perturbation exhibits relatively little sensitivity to the perturbation wavelength for higher wavelength and becomes more sensitive when $\lambda/L < 1$. For the pressure perturbation however, there exists a wavelength which allows for a local minimum in the perturbation value for the vdW gas. The shock transfer properties are not only affected by the non-ideal effects linked to the proximity to the thermodynamic critical point but also by the non-uniformity of the base-flow either side of the shock. The shock displacement, shown in Fig. 4 (right), varies significantly between ideal and vdW gases. The shock displacement in the vdW case is greater than that in the ideal gas case over most of the range of wavelengths presented with $|x'_{s,vdw}|/|x'_{s,ig}| \approx 10$ at $\lambda/L = 100$. The vdW shock displacement features a strong minimum around $\lambda/L \approx 0.15$ causing the magnitude to drop below that of the ideal gas. Transfer functions with slightly different mass flows through the nozzle (maximum $\Delta\dot{m}/\dot{m}_{M_1=1.1} \approx 9\%$ for $M_1 = 1.2$) are included in Fig. 4 to demonstrate the sensitivity of the results to this parameter. The pressure perturbation transfer function is the quantity that presents the strongest sensitivity to mass flux around the point where $|p'_2|$ undergoes a local minimum.

4   Comparison to DNS

In this section, we compare the results obtained via linear analysis to those obtained by solving the non-linear equations when the perturbation amplitude is small (referred to as DNS results). An example case for the vdW gas is chosen
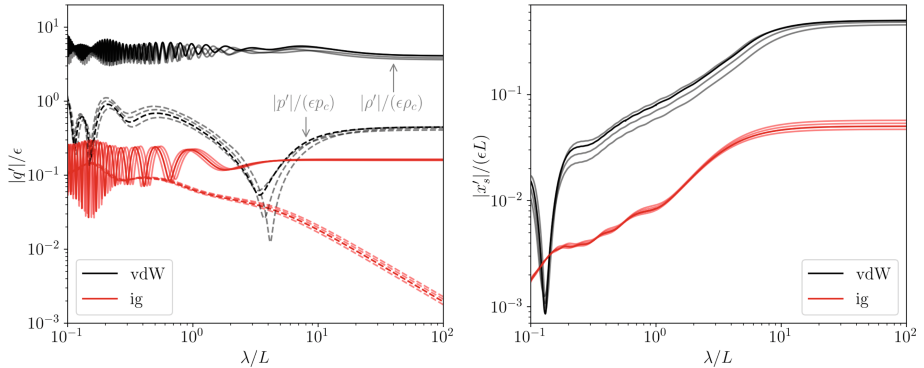
Fig. 4. (Left) modulus of the transfer function where solid and dashed lines are for $|\rho_2'/\epsilon|$ and $|p_2'/\epsilon|$ respectively and (Right) shock displacement magnitude for various length-scale ratios (non-reflective outlet and no outlet forcing) in red for ideal gas, black for vdW gas. The pre-shock conditions are: $p_a/p_c = 0.13$, $T_a/T_c = 1$ and $M_a = 3.1$ (obtained for $M_1 = 1.1$). The exit conditions are $p_2/p_c \approx 1.30$ for the ideal gas case and $p_2/p_c \approx 1.29$ for the vdW gas case. Lightly transparent curves are for slightly different mass flows ($M_1 \in \{1.05, 1.15, 1.2\}$) to illustrate sensitivity of the results to this parameter.

for comparison: for $\gamma = 1.013$, the upstream shock values are set to $M_a = 3.1$, $p_a/p_c = 0.13$ and $T_a/T_c = 1$ for an inlet Mach number $M_1 = 1.1$ i.e. the case of Fig. 4. The non-linear solver integrates Eq. 1 in time. First, a base-flow $\mathbf{q}_b$ is converged in time to a chosen precision. Then, an inlet density perturbation is prescribed at a given frequency ω (to match the desired λ/L value) and a sufficiently small amplitude ϵ (taken to be $\epsilon = 4 \times 10^{-3}$). The solution is advanced in time until a harmonic state is achieved giving the instantaneous perturbed flow denoted by $\mathbf{q}_n(t)$. For the following results, the comparison is carried out from $t = 10\tau$ (where τ is the period of the inlet perturbation) when the behaviour is expected to be harmonic. The numerical results plotted in Fig. 5 are thus $\mathbf{q}_n(t) - \mathbf{q}_b$ for $t \in [10\tau, 11\tau]$. The numerical integration is carried out using a 3rd order Runge–Kutta scheme for time integration and 4th order, 5 point-stencil centered finite difference scheme to calculate spatial derivatives. The computational space is discretised using $n_x = 5.6 \times 10^4$ points in order to resolve the shock displacement (the required number of points being estimated using the linear results and verified *a posteriori*). A constant and uniform artificial bulk viscosity is used to capture the discontinuity and tuned to ensure a scale separation between shock-thickness and perturbation wavelength while simultaneously damping the spurious oscillations at the shock (an approach used and validated in e.g. [1,7]). The inlet and outlet boundary conditions are enforced using a characteristic formulation for an arbitrary gas (see e.g. [5]). The results of Fig. 5 demonstrate the validity of the analysis in the linear regime – here for $\epsilon \sim 10^{-3}$ – as both the magnitude and phase of the shock displacement as well as the spatial distribution of ρ' are accurately recovered. The spatial distribution of the

density perturbation illustrates how the shock amplifies the density perturbation and compresses its associated wavelength.
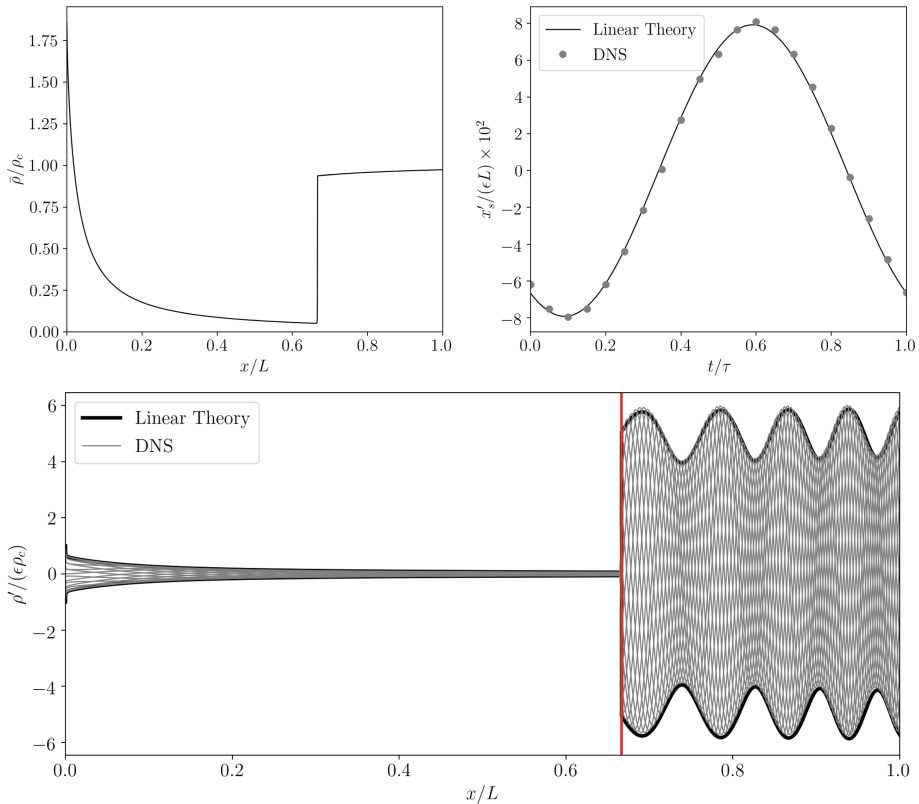

Fig. 5. Comparison of linear theory results to DNS results for a van der Waal gas for $t \in [10\tau, 11\tau]$. Top left: base-flow density distribution from DNS calculation with the shock located at $\bar{x}_s/L = 2/3$. Top right: relative shock displacement over time. Black lines for linear results and grey dots for DNS results. Bot.: spatial distribution of the density perturbation for an inlet entropy perturbation at $\lambda/L = 1$, the thick black line denotes the modulus of the perturbation resulting from the linear theory and the thin grey lines are the results from the DNS at various $t \in [10\tau, 11\tau]$. The red line denotes the mean shock position.

5   Conclusion

Initial results concerning non-ideal effects in a both shock-free and shocked supersonic diffuser have been presented here. In the shock-free case, integration of the linearised equations revealed a different redistribution of the inlet density perturbation across the primitive variables in the vdW case compared to the ideal

gas case allowing for a stronger pressure perturbation at the outlet of the nozzle at large wavelengths (compared to the nozzle length). This illustrates that the expansion through the nozzle itself, for a change of equation of state, is a first means of redistribution of the initial inlet perturbation across the primitive variables when compared to an ideal gas. For the case of shocked flow, the shock chosen in Sect. 3.2 further illustrates the importance of the equation of state in the redistribution of incoming primitive variable perturbations as the density perturbation is selectively amplified through this shock. Furthermore, for the conditions chosen in Sect. 3.2, the shock displacement is, over most of the wavelength range, an order of magnitude greater in the vdW case than in the ideal gas case. Such an increase in the displacement could lead to greater aerothermal loads on the divergent (e.g. in the case of shocks between turbine blades operating in a comparable region of $(p\text{-}\vartheta)$-space such as those of [6]). The impact of the outlet condition and possible upstream propagating acoustic waves have yet to be explored. For the latter, a possible resonance (or anti-resonance) of the shock displacement could be achieved by tuning the phase of an imposed upstream propagating acoustic forcing at the outlet.

References

1. Alferez, N., Touber, E.: One-dimensional refraction properties of compression shocks in non-ideal gases. J. Fluid Mech. **814**, 185–221 (2017)
2. Duran, I., Moreau, S.: Solution of the quasi-one-dimensional linearized Euler equations using flow invariants and the Magnus expansion. J. Fluid Mech. **723**, 190–231 (2013)
3. Goh, C.S., Morgans, A.S.: Phase prediction of the response of choked nozzles to entropy and acoustic disturbances. J. Sound Vibr. **330**(21), 5184–5198 (2011)
4. Guardone, A., Vimercati, D.: Exact solutions to non-classical steady nozzle flows of Bethe-Zel'dovich-Thompson fluids. J. Fluid Mech. **800**, 278–306 (2016)
5. Okong'o, N., Bellan, J.: Consistent boundary conditions for multicomponent real gas mixtures based on characteristic waves. J. Comput. Phys. **176**(2), 330–344 (2002)
6. Romei, A., Vimercati, D., Persico, G., Guardone, A.: Non-ideal compressible flows in supersonic turbine cascades. J. Fluid Mech. **882** (2020)
7. Touber, E., Alferez, N.: Shock-induced energy conversion of entropy in non-ideal fluids. J. Fluid Mech. **864**, 807–847 (2019)